Moving a Phenol Hydroxyl Group from the Surface to the Interior of a Protein: Effects on the Phenol Potential and pK_A[†]

Sam Hay,[‡] Kristina Westerlund,[‡] and Cecilia Tommos*

Department of Biochemistry and Biophysics, Arrhenius Laboratories for Natural Sciences, Stockholm University, SE-106 91 Stockholm, Sweden

Received May 14, 2005; Revised Manuscript Received July 6, 2005

ABSTRACT: De novo protein design and electrochemistry were used to measure changes in the potential and pK_A of a phenol when its OH group is moved from a solvent-exposed to a sequestered protein position. A "phenol rotation strategy" was adopted in which phenols, containing a SH in position 4, 3, or 2 relative to the OH group, were bound to a buried protein site. The α_3C protein used here is a tryptophan to cysteine variant of the structurally defined α_3W protein (Dai et al. (2002) *J. Am. Chem. Soc. 124*, 10952−10953). The protein characteristics of α_3C and the three mercaptophenol-α_3C (MP-α_3C) proteins are shown to be close to those of α_3W. Moreover, the phenol OH group is fully solvent exposed in 4MP-α_3C and more sequestered in 3MP-α_3C and 2MP-α_3C. Here we compare the redox properties of the three mercaptophenols when bound to α_3C and to cysteine free in water. The pK_A and E_{peak} values are essential identical when 4MP is ligated to α_3C relative to when it is free in solution. In contrast, these values are increased in 3MP-α_3C and 2MP-α_3C relative to the solvated compounds. The E_{peak} vs pH plots all display a ∼59 mV/pH unit dependence. We conclude that interactions with the OH group dominate the phenol redox characteristics. In 3MP-α_3C and 2MP-α_3C, hydrogen bonds between the protein and the bound phenols appear to either stabilize the reduced phenol or destabilize the radical, relative to the aqueous buffer, raising the potential by 0.11 and 0.12 V, respectively.

Essentially nothing is known about the reduction potentials of tyrosyl radicals in proteins. This is despite the number and importance of the enzymes employing tyrosine redox chemistry in biology (*1*−*5*). Thus, it is well-established that tyrosyl radicals are an integral part of the catalytic machinery in the class I ribonucleotide reductases (*6*−*8*) and in the light driven water-splitting chemistry catalyzed by photosystem II (*9*, *10*). Likewise, the properties of the cross-linked Tyr-Cys redox cofactor in the active sites of galactose oxidase and glyoxal oxidase have been studied for years (*11*−*13*). Tyrosyl radical chemistry is critical for the ability of photosystem II to oxidize water to dioxygen, and it may also play an important role for the reverse reaction. The heme a_3/Cu_B active site of cytochrome *c* oxidase contains a cross-linked Tyr-His pair, which has been proposed to participate in the redox reactions associated with the catalytic reduction of dioxygen to water in respiration (*14*). The two isoforms of prostaglandin H synthase contain several redox-active tyrosines of which one is catalytically active (*15*, *16*). How and why radical migration occurs in the prostaglandin H synthase isoenzymes remains an area of intense investigation (*2*, *16*, *17*). Tyrosyl radical formation has been reported for a number of other heme proteins, including bovine liver catalase (*18*), linoleate diol synthase (*19*), turnip peroxidase isoenzyme 7 (*20*), catalase-peroxidases from *Mycobacterium tuberculosis* (*21*) and *Synechocystis* (*22*), and cytochrome P450cam (*23*), although the involvement of these residues in catalysis remains to be established. In addition, a number of FAD-containing enzymes appear to employ tyrosine redox chemistry. Thus, the formation of a tyrosyl radical has been detected during the photoactivation process of DNA photolyase from *Anacystis nibulans* (*24*, *25*), and optical spectral features consistent with oxidized tyrosine were recently observed in photoactivated samples of the *Arabidopsis thaliana* cryptochrome blue-light photoreceptor (*26*). Finally, a tyrosyl radical in equilibrium with a FAD semiquinone was recently reported for partially reduced human monoamine oxidase A (*27*).

In contrast to a fairly substantial body of work describing the structural and spectroscopic properties of redox-active tyrosines in proteins, virtually nothing is known experimentally about their reduction potentials (E_m values)[1] and how these values depend on the solution pH and the protein environment. To date there are only a few values reported in the literature. The reduction potentials of the two redox-active tyrosines in photosystem II, Y_D and Y_Z, have been estimated at 0.74 ± 0.02 and 0.97 ± 0.02 V vs NHE, respectively (*28*). These numbers were derived by measuring equilibrium constants between several of the redox cofactors in the photosystem II electron-transfer chain and fixing the

[†] This work was funded by the Swedish Research Council and the Carl Trygger Foundation. S.H. was supported by a postdoctoral fellowship from the Wenner-Gren Foundation (Stiftelsen Wenner-Grenska Samfundet).

* To whom correspondence should be addressed. Phone: +46-8-162446. Fax: +46-8-155597. E-mail: cecilia@dbb.su.se.

[‡] These authors contributed equally to this work.

[1] Abbreviations: bCys, *N*-acetyl-L-cysteine methyl ester; DPV, differential pulse voltammetry; DTT, dithiothreitol; E_m, reduction potential; E_{peak}, DPV peak potential; Gdn:HCl, guanidine:HCl; MP, mercaptophenol; NHE, normal hydrogen electrode; P_i, phosphate buffer.

10.1021/bi050901q CCC: $30.25
Published on Web 08/12/2005

calculated ΔE_m values to the −0.13 V potential measured for Q_A/Q_A^-. The equilibrium constants and the Q_A/Q_A^- value were collected from different studies, and therefore, the exact experimental conditions, including the pH, to which the estimated Y_D and Y_Z potentials correspond are not clearly defined. Silva et al. made an attempt to measure the reduction potential of the redox-active Tyr-122 in *Escherichia coli* ribonucleotide reductase by spectroelectrochemical titration (*29*). The radical site in this enzyme is highly sequestered, and, even after extended incubation periods, only six of the 16 redox mediators included in this study were reported to interact with Tyr-122. Of these six mediators, five (with E_m in the range of 0.341−0.724 V) reduced the oxidized species to various degrees and one (E_m = 1.33 V) gave rise to a slight oxidation of Tyr-122 in its reduced form. The poor contact between the bulk medium and the radical site prevented a true equilibrium potential from being determined. The authors estimated an apparent potential of 1.0 ± 0.1 V for the Y•(122)/Y(122) redox pair at pH 7.6. Glyoxal oxidase and galactose oxidase operate at lower potentials, which has facilitated characterization of the redox active cysteine cross-linked tyrosinate in these two enzymes. The E_m value for radical formation in glyoxal oxidase was determined to be 0.64 V at pH 7.0 (*12*). Sykes and co-workers have used kinetic and spectroelectrochemical methods to investigate how the potential of the radical cofactor in galactose oxidase depends on different structural motifs in the active site (*30*−*32*). Galactose oxidase contains a copper ion coordinated by Tyr-272, Tyr-495, His-496, His-581, and an exogenous ligand (*33*−*35*). In addition, the indol headgroup of Trp-290 is closely associated with the thioether bond of the Tyr-272 and Cys-228 pair (*35*). For the wild-type system with OH^- at the exogenous site, the E_m value of the Y•(272)/Y^-(272) couple is 0.40 V at pH 7.5 (*30*). The potential is pH-dependent, increasing from 0.38 V at pH 8.5 to 0.50 V at pH 5.5, which was attributed to arise from acid/base reactions occurring at Tyr-495. For the Y495F mutants, a pH-independent value of 0.425 V was obtained. As a comparison, the peak potential of blocked tyrosine free in solution is 0.91 V at pH 5.5, 0.80 V at pH 7.5, and 0.74 V at pH 8.5 (*36*). Upon changing Trp-290 to a His, an increase in the Y•(272)/Y^-(272) potential to 0.73 V at pH 7.5 is observed (*31*). In apo-galactose, the E_m value of the Cys cross-linked Tyr radical cofactor is 0.57 V at pH 7.5 (*32*).

In photosystem II (*10*, *37*−*40*), other radical enzymes (*3*, *7*, *8*, *17*), and small molecule (e.g. *41*−*45*) and protein (*36*, *46*, *47*) model systems, the redox properties of tyrosine appear to be strongly influenced by the microenvironment surrounding the phenol OH group. To gain better insights on this issue, we have used de novo protein design and differential pulse voltammetry (DPV) to investigate how varying the degree of solvent accessibility to the hydroxyl group of a phenol influences its pK_A and DPV peak potential values. Our study is based on α_3C, which is a 7.5 kDa single-stranded protein designed to fold into a three-helix bundle with a unique Cys residing within the hydrophobic core. Via this residue, the tyrosine analogues 4-mercaptophenol, 3-mercaptophenol, and 2-mercaptophenol were covalently attached to α_3C by disulfide linkage. The position of the protein-anchoring sulfur group (4, 3, and 2) relative to the position of the hydroxyl group (*1*) in the three protein-ligated phenols is shown in Figure 1. By attaching the differently substituted mercaptophenols to Cys-32, the phenol OH group was rotated from a position at the protein surface toward more solvent-shielded positions in the interior of the protein. Here we describe a structural and electrochemical characterization of the mercaptophenol-α_3C proteins. To isolate the effects of the protein matrix on the phenol redox properties, the data derived from the protein samples are compared to data derived from the three mercaptophenols when bound to an uncharged blocked cysteine derivative in aqueous buffer.

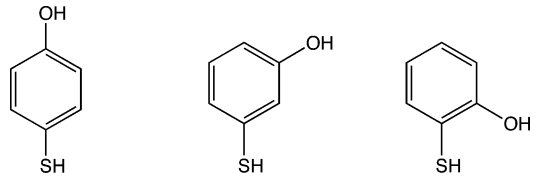

4MP 3MP 2MP

FIGURE 1: Schematic structures of 4-mercaptophenol (4MP), 3-mercaptophenol (3MP), and 2-mercaptophenol (2MP).

MATERIALS AND METHODS

Preparation of Mercaptophenol-Protein Samples. A gene encoding the α_3C protein was constructed by successive PCR of contiguous primers, sequenced, ligated into a pET11a expression vector, and transformed into *E. coli* BL21(DE3)LysS (Novagen). The α_3C gene encodes the following sequence: MTRVKALEEKVKALEEKVKALGGGGRIEELKKKCEELKKKIEELGGGGEVKKVEEEVKKLEEEIKKL, which is based on the α_3W and α_3Y proteins described in Tommos et al. (*36*) and Dai et al. (*48*). The α_3C sequence differs in the addition of a Thr at the N-terminus and the replacement of the lone Trp/Tyr at position 32 with a Cys. To keep the α_3C amino acid numbering consistent with the α_3W and α_3Y sequences, the additional N-terminal Thr is numbered here as −1. The expressed α_3C protein was purified from heat-treated cytosol (72 °C for 60 min) by gel filtration on a Superdex 30 HiLoad column (Pharmacia) followed by reversed phase HPLC on a semipreparative C18 column (Grace Vydac) using an acetonitrile/water/trifluoroacetic acid (Sigma ChromaSolv) gradient. The protein was lyophilized and then reduced with dithiothreitol (DTT; Saveen & Werner AB) in 3.0 M guanidine:HCl (Gdn:HCl), 30 mM KP_i, pH 8.0. The Gdn:HCl and DTT were removed by gel filtration (PD-10, Amersham Biosciences), and the protein concentration was immediately determined by Ellman's assay (Aldrich (*49*)) under denaturing conditions using an $\epsilon_{412\ nm}$ of 13.7 mM^{-1} cm^{-1}. The α_3C sample was split into four equal fractions and reacted with 3 mM 2-, 3-, or 4-mercaptophenol (MP; all purchased from Sigma) or DTT in 3.0 M Gdn:HCl, 10 mM KP_i, pH 8.0. The protein-to-phenol ratio was 1:5 in the reaction mixtures. The reactions were left to proceed at 4 °C overnight, and the Gdn:HCl and unbound mercaptophenol or DTT molecules were subsequently removed by PD-10 columns equilibrated with 10 mM KP_i, 100 mM KCl, pH 7.0. The protein concentration was determined from Ellman's assay of the DTT-reacted sample and assumed to be equal for all four samples.

Preparation of Mercaptophenol-N-acetyl-L-cysteine Methyl Ester Samples. The blocked cysteine analogue, *N*-acetyl-L-

cysteine methyl ester (bCys), was purchased from Sigma. Seven milligrams of bCys was added to 1 mL of a 1 mM NaOH solution containing 10 mM 2-, 3-, or 4-MP and reacted overnight at 20 °C. The bCys-MP compounds were isolated from the reaction mixtures on a reversed phase analytical C18 (Grace Vydac) column using a 20−70% acetonitrile in 50 min, acetonitrile/water/trifluoroacetic acid gradient. At a flow rate of 1 mL/min, the retention time of the bCys-MP compounds was ~11 min. The yield of bCys-MP ranged from 20% to 40% of the total amount of MP added.

NMR Spectroscopy. 1D NMR spectra were recorded on a Varian 500 MHz Inova spectrometer at 20 °C. The proteins were dissolved at ~0.85 mM in a 50 mM KP_i pH 6.0 buffer containing 30 mM KCl and 10% D_2O.

Electrochemical Measurements. Differential pulse voltammetry measurements were made essentially as described previously (*36*) using an AUTOLAB PGSTAT12 potentiostat equipped with a conventional three-electrode glass cell containing a 2 mm diameter glassy carbon working electrode, a platinum wire counter electrode, and a Ag/AgCl (3.0 M NaCl) reference electrode. The glass cell and the electrodes were purchased from Princeton Applied Research or Bioanalytical Systems (West Lafayette, IN). The measurements were performed in a 10 mM KP_i and 100 mM KCl buffer at room temperature under an argon atmosphere. The pH was continuously monitored in the cell (MI-414-6cm pH combination electrode, Microelectrodes Inc.) and adjusted with 1 M stocks of HCl and KOH. All peak potential data is referenced to the normal hydrogen electrode (NHE) by E_{peak}-(Ag/AgCl) + 0.196 V.

RESULTS

Protein Design. The design of the mercaptophenol-α_3C constructs is based on the properties of α_3W and α_3Y. These stable and uniquely structured de novo proteins contain a single buried Trp (α_3W) or Tyr (α_3Y) at position 32 (*36*, *48*). In α_3C, the aromatic side chain at position 32 was changed to a Cys to provide an anchor at which to covalently attach 4-mercaptophenol (4MP), 3-mercaptophenol (3MP), or 2-mercaptophenol (2MP) via a disulfide bond. Figure 2 shows a ribbon diagram of the α_3W NMR structure (A) and molecular models of α_3C with the three different MP molecules covalently bound to Cys-32 (B−D). The molecular model of 4MP-α_3C predicts that the phenol hydroxyl group will be at the surface of the protein and highly solvent exposed (Figure 2B). In contrast, in models of 3MP-α_3C (Figure 2C) and 2MP-α_3C (Figure 2D) the phenol hydroxyl group is predicted to reside in positions that are more sequestered from the solvent. As illustrated in Figure 2, the aim of the MP-α_3C designs was to create a model system in which to systematically change the microenvironment of the phenol OH group from a solvent exposed to a more sequestered milieu.

Binding of Mercaptophenols to α_3C. The NMR structure of α_3W shows that the accessible surface area of Trp-32 is <3% (*5*, *48*). The corresponding Cys-32 residue in α_3C is therefore predicted to be significantly shielded from the bulk phase. Consistent with this, α_3C cross-links slowly on the hour to day time scale (data not shown). To efficiently bind the mercaptophenol compounds to α_3C, ligation reactions

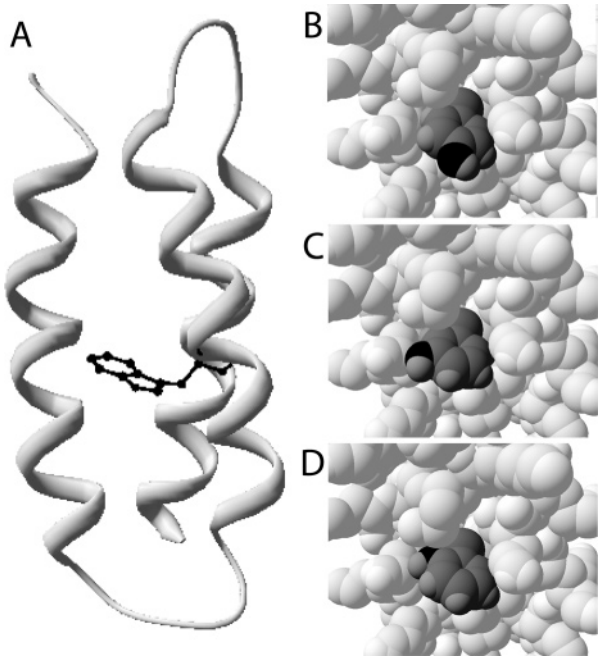

FIGURE 2: Modeling the structures of the α_3C-mercaptophenol adducts. (A) Ribbon diagram of the experimentally determined solution structure of α_3W (pdb file 1LQ7) upon which the models are based. The structure was solved using multidimensional NMR methods to an all heavy atom RMSD precision of 1.29 ± 0.11 Å (*48*). Models of the mercaptophenol-α_3C proteins were obtained by restrained energy minimization of the mean structure of α_3W using Swiss-PdbViewer version 3.7 (*74*). Partial space filling representations of the site of attachment of 4MP, 3MP, and 2MP are shown in panels B, C, and D, respectively. The mercaptophenols are shown in dark gray with their phenol oxygen atom displayed in black.

were carried out under fully denaturing conditions with a 5-fold molar excess of MP over protein. The three different MP/α_3C ligation mixtures, and one α_3C sample in which MP was replaced with DTT, were prepared in parallel using equal amounts of a common α_3C protein stock. In addition, a 2MP control sample was prepared to which no protein was added. Following an overnight incubation, unbound denaturant and MP or DTT molecules were removed by gel filtration and the samples exchanged into a benign buffer promoting the folding of the α_3C proteins. As described below, the ligation reactions were monitored by UV/vis absorption spectroscopy, analytical reversed phase HPLC, and mass spectrometry and are shown to occur with high efficiency. Furthermore, no unbound MP was detected in any of the samples.

Figure 3A shows the absorption spectra of the 2MP (protein-free) control sample described above (spectrum a), 2MP free in buffer (spectrum b), and the 2MP-reacted α_3C sample (spectrum c). Spectrum a, representing the protein-free 2MP control sample after gel filtration, shows a complete lack of absorbance. This confirms that unbound mercaptophenol molecules were removed from the solution of the overnight-incubated samples in the buffer-exchange step.

The absorption spectra of 2MP in solution (spectrum b) and of the 2MP-reacted α_3C sample (spectrum c) were both obtained at pH 7.0 and correspond to the protonated phenol species (vide infra). In the spectrum representing the freely dissolved phenolic compound, absorption maxima are observed at 256 and 295 nm. In the spectrum of the 2MP-

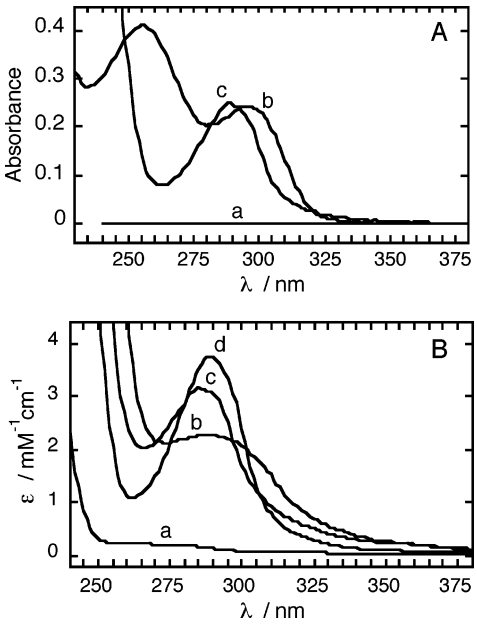

FIGURE 3: (A) UV/vis absorption spectral analysis of the 2-mercaptophenol/α_3C ligation reaction. Spectrum a represents a control measurement of the buffer-exchange step performed in the ligation protocol (see text for details). Spectrum b represents 2MP dissolved in a 50 mM KP_i pH 7.0 buffer and spectrum c the 2MP-reacted α_3C sample diluted in the same buffer. (B) Absorbance spectrum of (a) unlabeled α_3C, (b) 4MP-α_3C, (c) 3MP-α_3C, and (d) 2MP-α_3C. The proteins were dissolved in a 10 mM KP_i and 100 mM KCl pH 7.0 buffer. All spectra were collected on a Varian Cary 4 spectrophotometer at room temperature using a 1 cm path length cuvette. The four samples were estimated to contain 185 μM protein based on Ellman's assay of the unreacted α_3C sample (see text).

reacted α_3C sample, these absorption bands have shifted to shorter wavelengths. Spectrum c exhibits a weak shoulder around 244 nm indicating the presence of one of the absorption bands that now overlaps with the strong absorption of the protein backbone. The second absorption band occurs in the aromatic spectral region and has an absorption maximum at 289 nm. The large differences, with respect to both position and spectral line shape, between the 2MP solution spectrum and the spectrum of the 2MP-reacted α_3C sample indicate that the mercaptophenol has ligated to the protein.

Spectrum a in Figure 3B shows the absorption of the DTT-treated α_3C sample. α_3C contains no aromatic residues, and consequently the protein absorbs very weakly in the aromatic spectral region. This makes the UV/vis absorption spectral analysis insensitive in detecting any potential contamination of unlabeled protein in the 2MP-reacted α_3C sample. Analytical reversed phase C18 HPLC measurements were performed to address this issue. Figure 4A shows an HPLC trace of the DTT-treated α_3C sample to which no phenol addition had been made. The elution of the protein was monitored at 220 and 289 nm. The 220 nm absorption trace shows two partly resolved peaks representing α_3C with and without the N-terminal methionine. The partial posttranslational removal of the initiator Met from the expressed α_3C protein was confirmed by mass spectrometry (m/z = 7418 and 7549 ($\pm$0.5) Da at a ratio of approximately 1:3, data not shown). There are no 289 nm absorption changes observed in the elution profile of α_3C, consistent with this protein having no significant absorption at this wavelength (Figure 3B, spectrum a). Figure 4B shows a corresponding

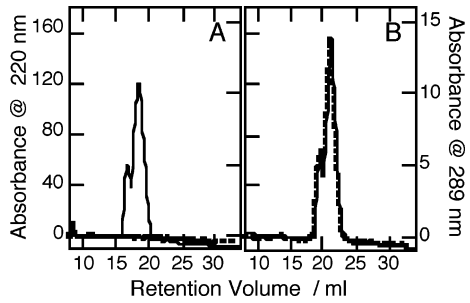

FIGURE 4: HPLC analysis of the 2-mercaptophenol/α_3C ligation reaction. (A) Elution profile of the DTT-reacted α_3C sample. (B) Elution profile of the 2MP-reacted α_3C sample. The eluted proteins were monitored at 220 nm (solid line, protein backbone and 2MP absorbance) and 289 nm (dotted line, 2MP absorbance). The proteins were eluted on a reversed phase analytical C18 column using a 30−60% acetonitrile in 20 min acetonitrile/water/trifluoro acetic acid gradient.

HPLC trace of the 2MP-reacted α_3C sample. There are clear differences between the chromatogram representing α_3C and that of the 2MP-reacted α_3C sample. First, the retention volume of the eluted α_3C and 2MP-α_3C proteins differs by more than 4 mL. Second, the elution profile of the 2MP-reacted α_3C sample displays a perfect overlap between the 220 and 289 nm absorbance traces. This feature indicates that the 2MP-reacted α_3C sample does not contain unlabeled protein since the retention volume differs between α_3C and 2MP-α_3C. Thus, a sample containing a mixture of α_3C with and without the phenol ligand is predicted to show an elution profile in which the 220 nm absorbance, which represents both α_3C and 2MP-α_3C, gives rise to a broader peak than the 289 nm absorbance, which is detecting only 2MP-α_3C. This conclusion, made on the basis of the HPLC data, was confirmed by MALDI mass spectrometry measurements. For the 2MP-α_3C ligation sample, the m/z were 7451.5, 7671.5, and 7688.5 Da ($\pm$1 Da; data not shown), corresponding to 2MP-α_3C, 2MP-α_3C with the N-terminal Met, and a water adduct of the 2MP-α_3C-Met protein, respectively. No trace of unlabeled α_3C was detected in the mass spectrometry data. In addition, no contribution of free 2MP was detected by the mass spectrometry analysis of the 2MP-reacted α_3C. This result showed that there was no unspecific binding of the phenolic molecule to the surface of α_3C.

Analytical reversed phase C18 HPLC analyses of the 3MP-α_3C and 4MP-α_3C ligation samples showed the same characteristics, with an increase in the retention volume relative to α_3C and an exact overlap between the 220 and 289 nm absorbance traces (data not shown), as observed for the 2MP-reacted α_3C sample (Figure 4). We conclude that the ligation protocol used here generated homogeneous mercaptophenol-α_3C protein samples.

The high efficiency of the ligation protocol allowed us to estimate the extinction coefficients of the protein-ligated MP compounds. The near-UV absorption spectra of α_3C and the mercaptophenol-α_3C protein samples are shown in Figure 3B. Their respective absorbance maximum and estimated extinction coefficient at 290 nm, ϵ_{290}, are given in Table 1. To obtain the ϵ_{290} values shown in Table 1, the protein concentration in the DTT-treated α_3C sample that was prepared in parallel with the mercaptophenol-α_3C samples was determined by using Ellman's reaction. This assay is used to detect the concentration of free thiol groups (*49*),

Table 1: Physical Properties of the α_3C and Mercaptophenol-α_3C Proteins[a]

protein	phenol λ_{max}	ϵ_{290}	$[\Theta]_{222}$	% helix[b]	% helix[c]	ΔG^{H_2O} [d]	m[d]
α_3C		0.1	23.3	71	72	−4.1 (0.2)	2.1 (0.1)
4MP-α_3C	247, 288	2.3	27.5	81	85	−3.7 (0.2)	1.5 (0.1)
3MP-α_3C	285	3.1	28.1	83	87	−3.1 (0.1)	1.2 (0.1)
2MP-α_3C	289	3.7	26.1	78	81	−3.1 (0.2)	1.2 (0.1)

[a] Units: λ_{max}, nm; ϵ_{290}, mM^{-1} cm^{-1}; $[\Theta]_{222}$, mdeg cm^2 $dmol^{-1}$ $residue^{-1}$; ΔG^{H_2O}, kcal mol^{-1}; m, kcal mol^{-1} M^{-1}. [b] Calculated by the method of Sönnichsen et al. (*75*) by $[\Theta]_{222\,nm} = [\Theta]^{\infty}_{helix}((\%\ helix/100) - ik/n)$, where $[\Theta]^{\infty}_{helix}$ is −39.5 mdeg cm^2 $dmol^{-1}$ for an infinity long α-helix, k is 2.57 at 222 nm (*76*), i is 3, the number of individual α-helices, and n is 66, the number of amino acids. [c] Scaled relative to α_3W, which has a $[\Theta]_{222}$ value of −24.6 mdeg cm^2 $dmol^{-1}$ $residue^{-1}$ and is 76% α-helical as judged from the NMR structure of Dai et al. (*48*). [d] Calculated from the pH 7.5 Gdn:HCl denaturation data shown in Figure 5B. Values in parentheses are the error obtained from fitting the data. Under the same conditions, α_3W has a ΔG^{H_2O} value of −3.3 (0.1) kcal mol^{-1} and m value of 1.9 (0.1) kcal mol^{-1} M^{-1} (data not shown).

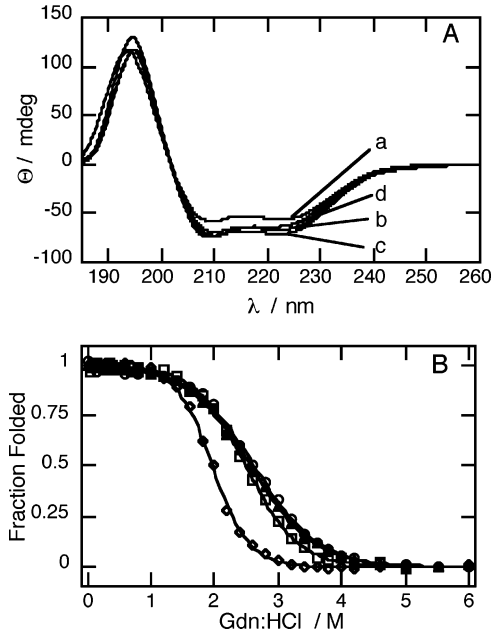

FIGURE 5: (A) Circular dichroism spectra of (a) α_3C, (b) 4MP-α_3C, (c) 3MP-α_3C, and (d) 2MP-α_3C. (B) Guanidine:HCl denaturation of α_3C (diamonds), 4MP-α_3C (squares), 3MP-α_3C (triangles), and 2MP-α_3C (circles). The loss in secondary structures as a function of denaturant concentration was followed by monitoring the CD intensity at 222 nm. The solid lines are a fit to the data using the method of Santoro and Bolen (*50*). The derived ΔG^{H_2O} and m values are given in Table 1. The data were collected on a JASCO-720 spectropolarimeter at 23 °C using a 0.1 cm path length cuvette. The proteins were dissolved at 37 μM in a 10 mM KP_i and 15 mM KCl pH 7.5 buffer. The α_3C sample contained 1 mM DTT to prevent cross-linking of the protein.

and it was performed under fully denaturing conditions. Assuming that the protein concentration was the same in the four parallel-processed samples, the extinction coefficients shown in Table 1 were calculated from the absorbance of the mercaptophenol-α_3C samples.

Characterization of the Unlabeled and Mercaptophenol-Labeled α_3C Proteins. Figure 5A shows the far-UV CD spectra of α_3C in the absence and presence of bound 4MP, 3MP, and 2MP. The protein spectra are all characteristic of α-helical structures displaying a maximum at about 195 nm and minima at 208 and 222 nm. The degree of α-helicity for the four proteins was calculated from the intensity at 222 nm of each CD spectrum. The α-helical content of α_3C was estimated to be 71%. This value increased to 81%, 83%, and 78% for 4MP-α_3C, 3MP-α_3C, and 2MP-α_3C, respectively. A second method to estimate the degree of α-helical content in the α_3C proteins was to compare their CD spectra to the spectrum of α_3W, which represents a three-helix bundle with a known α-helical content of 76% (*48*). By comparing the mean residue ellipticity value at 222 nm, $[\Theta]_{222}$, for all five proteins, the degree of α-helicity increased by 1% to 4% for the four α_3C proteins relative to the calculated numbers. The $[\Theta]_{222}$ and the α-helical content of α_3C and the three mercaptophenol-α_3C proteins are given in Table 1. We conclude that mercaptophenol ligation to α_3C does not disrupt the formation of secondary structures and that 4MP-α_3C, 3MP-α_3C, and 2MP-α_3C have α-helical contents that are close to that of the well-characterized α_3W three-helix bundle protein. Consistent with the CD characterization, 1D NMR spectra of α_3C and the labeled proteins display spectral features similar to those of α_3W and typical of a structured helical protein with backbone H^{α} resonances centered at 4.05 ppm and a chemical-shift dispersion in the amide region of ∼2.0 ppm (data not shown (*36*)).

The effect of MP binding on the protein stability was examined by monitoring the loss of secondary structure in α_3C and the three mercaptophenol-ligated α_3C proteins as a function of guanidine:HCl (Gdn:HCl) concentration. Denaturation plots of the four proteins obtained at pH 7.5 are shown in Figure 5B. The data were fitted using the method described by Santoro and Bolen (*50*), and the derived free energy of unfolding, ΔG^{H_2O}, and m values are given in Table 1. α_3C has a stability of −4.1 kcal mol^{-1}, and it unfolds in a highly cooperative manner. This is evident by the steep slope of the α_3C Gdn:HCl denaturation plot providing an m value of 2.1 kcal mol^{-1} M^{-1}. The α_3C protein is 0.8 ± 0.2 kcal mol^{-1} more stable than the original α_3W protein, which has ΔG^{H_2O} and m values of −3.3 kcal mol^{-1} and 1.9 kcal mol^{-1} M^{-1}, respectively, at pH 7.5 (Table 1). This increase in stability could arise from a slight repacking of the hydrophobic core as the bulky indole side chain of Trp-32 is replaced with the smaller side chain of Cys-32. In addition, helical propensity values predict an increase in stability by 0.23 to 0.44 kcal mol^{-1} when changing a Trp to a Cys (*51*, *52*). Upon binding 4MP to α_3C, the protein stability and the cooperativity of the unfolding event are somewhat lowered to a ΔG^{H_2O} value of −3.7 kcal mol^{-1} and an m value of 1.5 kcal mol^{-1} M^{-1}. When the ligated phenol is exchanged from 4MP to 3MP or 2MP, the protein stability decreases by a further 0.6 kcal mol^{-1} and the m value by 0.3 kcal mol^{-1} M^{-1}. The −3.1 kcal mol^{-1} M^{-1} stability value of 3MP-α_3C and 2MP-α_3C are close to the −3.3 kcal mol^{-1} M^{-1} value of α_3W. We conclude that α_3C and the three MP-ligated α_3C proteins are all helical and folded in solution.

The molecular model of 4MP-α_3C predicts that the phenol hydroxyl group is solvent accessible (Figure 2B). In contrast, in the structural models of 3MP-α_3C and 2MP-α_3C the phenol hydroxyl group is rotated away from the surface toward the interior of the protein (Figure 2C,D). The core of the three-helix bundle proteins consists of nonpolar residues including Leu, Ile, and Val. Solvating a polar hydroxyl group within this hydrophobic environment is

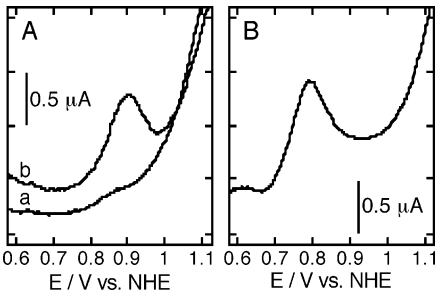

FIGURE 6: (A) Differential pulse voltammograms of (a) α_3C and (b) 2MP-α_3C. (B) Differential pulse voltammogram of *N*-acetyl-L-cysteine methyl ester-2-mercaptophenol (2MP-bCys). All samples were at a concentration of about 200 μM in a 10 mM KP_i and 100 mM KCl pH 7.0 buffer at room temperature. Experimental conditions: scan rate, 20 mV s^{-1}; modulation amplitude, 50 mV; step potential, 2 mV; modulation time, 2 ms; interval time, 100 ms.

expected to lower the stability of the protein. Thus, the drop in stability observed for the 2MP-α_3C and 3MP-α_3C proteins relative to 4MP-α_3C is consistent with the prediction made by the structural modeling.

Electrochemistry of the Mercaptophenol-Labeled α_3C Proteins. We have previously demonstrated the utility of differential pulse voltammetry (DPV) for the determination of potentials and pK_A values associated with the redox chemistry of Trp and Tyr resides both in solution and within a protein (*36*). This technique has also been used to measure the solution potentials of 3-nitrotyrosine (*53*), 2,3-difluorotyrosine (*54*), an aniline amino acid (*55*), and tyrosine covalently bound to a ruthenium tris-bipyridyl complex (*56*).

Differential pulse voltammograms of the unlabeled (trace a) and 2MP-bound (trace b) α_3C proteins are shown in Figure 6A. The reduction potential at pH 0, $E_{m,0}$, for an alkyl-$S^\bullet$ + H^+ + e^- = alkyl-SH half-reaction has been determined to be about 1.33 V (*57*). Assuming a 59 mV/pH unit dependence, we calculate an $E_{m,7}$ value of 0.92 V for the $Cys^\bullet$/Cys redox couple in solution. There was no detectable signal from the unlabeled α_3C protein at neutral pH (trace a) nor at acidic or alkaline conditions (data not shown). Either the protein matrix has shifted the potential of Cys-32 outside the measurable range ($\sim$1.3 V) and/or the lack of a signal is a kinetic effect due to the slow oxidation rate of thiols at the surface of a glassy carbon electrode (*58*). In contrast to α_3C, electrochemical signals were observed from the three different MP-ligated α_3C proteins. A typical voltammogram is shown in Figure 6A where trace b represents 2MP-α_3C at neutral pH. Two different redox reactions are expected to occur in the MP-α_3C proteins: reduction of the S$-$S bond or oxidation of the phenol headgroup. The E_m of the cystine/cysteine redox couple is predicted to be <0 V over the whole 4$-$10 pH range (*59*), which were the conditions used here for the characterization of the MP samples (vide infra). To avoid reduction of the Cys$-$MP bond, all electrochemical measurements were limited to potentials $\geq +0.2$ V. As a reference for 2MP ligated to α_3C, the phenolic compound was bound to the uncharged cysteine analogue *N*-acetyl-L-cysteine methyl ester and the resulting molecule (2MP-bCys) was characterized at the same conditions as the protein sample. The DPV trace of bCys-2MP obtained at pH 7.0 is shown in Figure 6B. As for unlabeled α_3C, free bCys without the mercaptophenol was electrochemically inert in the 0.2 to 1.3 V range used in this study (data not shown). We conclude that the voltammograms shown in Figure 6 represent oxidation of the 2MP moiety bound to α_3C (A; trace b) or bCys (B). The average width of the 2MP-α_3C and 2MP-bCys DPV peaks is 0.14 $\pm$ 0.03 and 0.10 $\pm$ 0.01 V, respectively, suggesting that the oxidation reactions were not reversible (fwhm = 0.089 V for an $n = 1$ reversible reaction at 21 °C (*60*)). Cyclic voltammetry measurements of 2MP-α_3C and 2MP-bCys gave irreversible traces, confirming this conclusion (scan rates 0.01$-$10 V s^{-1}; data not shown). For the MP samples studied here, the measured DPV peak widths were typically between 0.1 and 0.16 V. Electrochemical oxidation of Trp and Tyr is irreversible in solution since the secondary radical chemistry is fast relative to the time scale of the voltammetry experiment (*61*). However, the E_{peak} values derived from cyclic voltammetry and DPV measurements on Trp and Tyr (*36*, *61*) correlate closely to the equilibrium E_m values derived for these species using pulse radiolysis (*62*). We estimate that the E_{peak} values obtained from the DPV experiments equal $E_m \pm 0.02$ V (*36*).

The $E_{peak,7}$ values derived from the 2MP-α_3C and 2MP-bCys voltammograms in Figure 6 are 0.91 and 0.79 V, respectively. Thus the protein matrix elevates the 2MP potential by 0.12 V at pH 7.0. Similar experiments were performed with 3MP and 4MP (data not shown), and the resulting $E_{peak,7}$ values are given in Table 2. The potential of 3MP increases by 0.11 V when the phenol is ligated to α_3C relative to when it is bound to bCys. In contrast, there is no significant difference between the 4MP-α_3C and 4MP-bCys potentials at neutral pH. To further investigate the influence of the protein matrix on the redox properties of the phenolic compounds, the DPV experiments were extended to cover the whole pH 4 to 10 range. Peak potentials as a function of pH are shown in Figure 7 for 4MP (A), 3MP (B), and 2MP (C) bound to both α_3C and bCys. Tyrosine and phenol oxidation is expected to have a pH dependence described by the Nernst relationship:

$$E_m = E_m(PhO^\bullet/PhO^-) + \ln(10)RT/nF \log\left[1 + \frac{10^{-pH}}{10^{-pK_{red}}}\right] \quad (1)$$

where $E_m(PhO^\bullet/PhO^-)$ is the pH-independent reduction potential of the phenolate, and pK_{red} is the pK_A of the phenol/phenolate couple. At acidic and neutral pH values, all of the data in Figure 7 show the linear pH dependence that is characteristic of a coupled one-electron/one-proton redox reaction ($\ln(10)RT/nF \sim 0.059$ mV/pH unit at room temperature; values are given in Table 2). Thus upon oxidizing the ligated phenol in all three proteins, one full proton is released into the bulk medium.

At alkaline pH, the potentials of the three different MP-bCys compounds become pH-independent, allowing the measurement of the pK_{red} and $E_{peak}(PhO^\bullet/PhO^-)$ values. These values are given in Table 2. The electrochemical characteristics of the 4MP-α_3C protein are, considering their precision, essentially identical to those of the freely dissolved 4MP-bCys compound (Figure 7A; Table 2). This was not the case for the 3MP-α_3C and 2MP-α_3C proteins, where the pK_{red} values were found to be shifted to >10 (Figure 7A,B; Table 2). To confirm the acid/base properties of the reduced α_3C- and bCys-bound MP species by a second experimental

Table 2: Electrochemical Properties of 4-, 3-, and 2-Mercaptophenol Bound to α_3C and to *N*-Acetyl-L-cysteine Methyl Ester (bCys)[a]

species	pK_A	pK_{red}	$-\ln(10)RT/nF$	dE_{peak}(PhO•/PhO$^-$)	$E_{peak,7}$	$\Delta E_{peak,7}$
4MP-bCys	9.3	9.7 (0.1)	0.059 (0.001)	0.64	0.80	
4MP-α_3C	9.5	9.4 (0.1)	0.064 (0.002)	0.64	0.79	−0.01
3MP-bCys	9.6	9.8 (0.1)	0.059 (0.002)	0.79	0.96	
3MP-α_3C	>10	>10	0.058 (0.003)	nd[b]	1.07	0.11
2MP-bCys	9.0	8.8 (0.1)	0.060 (0.001)	0.69	0.79	
2MP-α_3C	>10	>10	0.057 (0.005)	nd[b]	0.91	0.12

[a] Values in parentheses are the error obtained from fitting the data in Figure 7. The error in pK_A values is better than ±0.1. All potentials are in units of V and are relative to the normal hydrogen electrode. The error in potentials is ±10 mV. [b] Not determined.

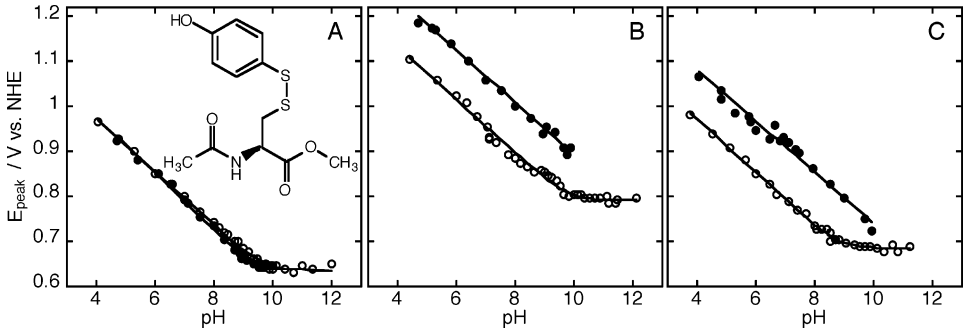

FIGURE 7: Differential pulse voltammetry (DPV) peak potentials (E_{peak}) as a function of solution pH for (A) 4MP, (B) 3MP, and (C) 2MP when bound to α_3C (closed circles) and to *N*-acetyl-L-cysteine methyl ester (bCys; open circles). The inset to panel A shows the chemical structure of *N*-acetyl-L-cysteine methyl ester-4-mercaptophenol (4MP-bCys). The solid lines represent fits using Equation 1. Fitting parameters are given in Table 2.

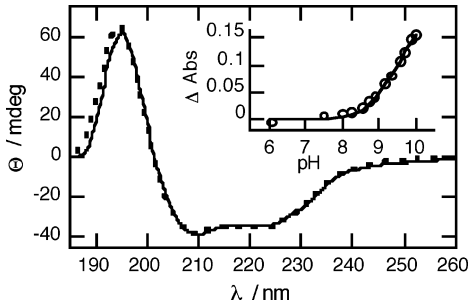

FIGURE 8: Circular dichroism spectra of 4MP-α_3C at pH 7.58 (solid line) and pH 9.94 (dotted line). The data were collected on a JASCO-720 spectropolarimeter at 23 °C using a 0.1 cm path length cuvette. The protein was dissolved at about 20 μM in a 10 mM KP_i and 10 mM KCl buffer. The inset shows the formation of the mercaptophenolate in the same protein as measured by change in absorbance at 305 nm. The solid line is a fit with a single pK_A of 9.5. The data were collected on a Varian Cary 4 spectrophotometer at room temperature using a 1 cm path length cuvette. The protein was dissolved at about 50 μM in a 10 mM KP_i and 100 mM KCl buffer.

technique, their pK_A values were investigated by pH titration of the phenolate absorbance (data not shown), and these values are also listed in Table 2. The bCys-bound MP pK_A values are in good agreement with their respective pK_{red} values. Additionally, the pH titration curve of 4MP-α_3C gave a pK_A value of 9.5 ± 0.1 (Figure 8, inset), which is in close agreement with the 9.4 ± 0.1 value derived from the DPV measurements. Furthermore, no phenolate absorbance was observed in either 3MP-α_3C or 2MP-α_3C at pH 9.9 (data not shown), which is consistent with the electrochemical measurements. Thus, for the 3MP and 2MP molecules, the protein milieu increases the pK_A value by >0.3 and >1.0 pK unit, respectively, relative to the solution values.

As predicted by the protein modeling and suggested by the DPV and pH titration data described above, the phenol OH group in 4MP-α_3C appears to be highly solvent exposed. To test this further, the pH dependence of the secondary structures of this protein was monitored by CD spectroscopy. Figure 8 shows CD spectra of 4MP-α_3C at pH 7.58 (solid line) and 9.94 (dotted line), and the inset shows the phenolate absorbance of the same protein as a function of pH. With a pK_A of 9.45, the phenol goes from protonated at pH 7.58 to a predominantly deprotonated state at pH 9.94, and yet there is no significant change in the protein CD spectrum. It is unlikely that a charge can be formed in the interior of α_3C, which contains no polar residues, without affecting its secondary structures to some extent. We conclude that when the protein-anchoring mercapto group is in the 4-position, the phenol OH group is at, or on the outside of, the protein surface.

DISCUSSION

Tyrosine-mediated electron transfer and proton-coupled electron transfer is emerging as a common functional theme in enzymes employing amino acids as catalytic redox cofactors. Great progress has been made with respect to characterizing the structural and spectroscopic properties of tyrosyl radical enzymes. In addition, innovative experimental approaches are breaking new ground and are broadening our knowledge of the chemistry occurring in these systems. For example, Stubbe, Nocera, and their co-workers have used intein technology to introduce nonnatural amino acids into *E. coli* ribonucleotide reductase to investigate at what residues protonic reactions are coupled to the electron transfer along the proposed radical-transfer chain (*53*−*55*). Nonetheless, systematic studies characterizing the thermodynamic properties of tyrosyl radicals in proteins are scarce, essentially nonexistent, in the literature. To the best of our knowledge, the only tyrosine redox cofactor that has been investigated in any detail is the radical-forming Tyr-272 in the active site of galactose oxidase (*30*−*32*), and this residue is unique since it is deprotonated in its reduced form, coordinated to

a metal, and cross-linked to a cysteine (*13*). The reason for this paucity of information about the basic chemistry of tyrosine redox cofactors is the simple fact that their reduction potentials typically are so high that the oxidation of bulk water, other cofactors or chromophores, and the protein matrix itself interferes with measurements. The "redox inert" design of the α_3W and α_3Y proteins was specifically directed to address this problem and make a protein model system suitable for investigating the properties of amino acid redox cofactors by electrochemistry and allow these measurements to be performed at high potentials and over a broad pH range (*5*, *36*). Briefly, α_3W and α_3Y are well-structured three-helix bundles with a hydrophilic surface dominated mainly by Glu and Lys residues and a protein core consisting of Val, Leu, and Ile amino acids together with a single aromatic residue at position 32 (Trp-32 in α_3W and Tyr-32 in α_3Y (*5*, *36*, *48*)). This position is the designated redox site, and the protein scaffold contains no other residues that are expected to have an E_m in the biological relevant range ($<\sim$1.2 V). An advantage of their fairly simple overall composition is that it facilitates spectroscopic characterization of these proteins. For example, changes in helical content as a function of pH, or some other parameter, can easily be monitored by CD spectroscopy and there are no complex spectral overlaps in their absorption and fluorescence spectra. Furthermore, α_3W and α_3Y are stable from pH 4 to 10 and this structural tolerance for relatively large changes in solution pH facilities characterization of the pH dependence of the redox reactions.

The goal of the work presented here is to investigate how, and to what degree, the potential and pK_A values of a phenol change when its hydroxyl group is moved from a solvent-exposed position to a more sequestered site surrounded by hydrophobic residues. To accomplish this, a "phenol rotation strategy" was adopted that consists of ligating phenols containing a chemical tag in the para (position number 4), meta (number 3), or ortho (number 2) position, relative to the phenol hydroxyl group (number 1), to a single site in the protein. For several reasons, we choose to test this strategy by using mercaptophenols. First, α_3C is a single-point mutant of the original α_3W and α_3Y proteins (Trp/Tyr-32 to Cys), and this mutation was predicted to impact the structural and pH properties of the three-helix bundle scaffold only to a minor extent. An important advantage of the MP compounds is that their facile ligation to α_3C provided homogeneous material for the protein characterization and electrochemical measurements. An additional benefit was that all of the three different monosubstituted phenols (Figure 1) were commercially available. We note that the focus of this work is not on the absolute potentials and pK_A values of the different MP molecules but on the *differences* in these values when the phenols are bound to α_3C relative to cysteine free in solution. For the solution measurements, a blocked cysteine (bCys; Figure 7A) was used to avoid any effects on the phenol potential and pK_A values arising from acid/base reactions occurring at the carboxyl and amino groups.

The structure of α_3C is based on the traditional helical-bundle design with apolar residues in the heptad *a* and *d* positions forming the main part of the hydrophobic core and polar residues in the remaining heptad *b*, *c*, *e*, *g*, and *f* positions forming the interhelical and fully exposed parts of the protein (*5*). The structural characterization of 4MP-α_3C gave no indications of large-scale structural changes relative to α_3C and α_3W, i.e., helical content, global stability, and NMR characteristics were similar for the three proteins (Figure 5; Table 1). The most reasonable conclusion is that the overall three-helix bundle topology is maintained in 4MP-α_3C and that residue 32, which is in a heptad *a* position, is turned toward the interior of the protein. We can also conclude from the structural characterization that the phenol hydroxyl group is fully solvent exposed (Figure 8; Table 2). It appears that the protein matrix is folded around the hydrophobic part of the 4MP molecule and that the phenol OH group is residing at or on the outside of the protein surface. As a comparison, in α_3W all of the carbon atoms associated with Trp-32 reside in the core while the polar NH group is oriented toward the protein surface (*5*, *48*).

Most interestingly, the redox properties of 4MP are essentially identical when the aromatic molecule is ligated to α_3C relative to when it is bound to bCys (Figure 7A; Table 2). Taking the average from the electrochemical and phenolate titration experiments provides a pK_A of 9.45 and 9.50 $\pm$ 0.1 for 4MP-α_3C and 4MP-bCys, respectively. The pH-independent E_{peak} value of the PhO$^{\bullet}$/PhO$^-$ redox couple equals 0.64 V for both 4MP-α_3C and 4MP-bCys. This suggests that the charge environment around the phenol hydroxyl group is very similar in the two systems and that the salt-containing aqueous buffer efficiently screens any electrostatic interactions between the phenol OH group in 4MP-α_3C and the surface of the protein. The pH-dependent part of the E_{peak} vs pH plots in Figure 7A represents the neutral PhO$^{\bullet}$/PhOH redox pair. The slope is 64 $\pm$ 2 and 59 $\pm$ 1 mV/pH unit for 4MP-α_3C and 4MP-bCys, respectively, which is consistent with a one-electron oxidation of the phenol to the phenoxyl radical state and the release of one full proton into the bulk medium. The phenol in 4MP-α_3C is partly buried inside the protein and clearly must experience a very different environment relative to the fully solvent-exposed phenol in 4MP-bCys, and yet their redox properties are remarkable similar. This suggests that the environment around the hydroxyl group is not merely important for tuning the redox properties of a phenol but, in fact, absolutely dominating.

When the phenol is bound to α_3C via the meta or ortho position, distinct differences are observed between the protein and the solution systems (Figure 7B,C; Table 2). The average phenol pK_A is calculated to 9.7 $\pm$ 0.1 for 3MP-bCys and 8.9 $\pm$ 0.1 for 2MP-bCys. These values increase to $>$10 when the phenols are bound to α_3C, which suggests that in both of the labeled proteins the phenol OH group has rotated away from the surface toward the apolar core. Solvating the polar OH group inside the hydrophobic interior of α_3C is expected to increase the phenol pK_A and lower the stability of the protein relative to the situation when the phenol OH group is solvent exposed. As shown in Figure 5B and Table 2, the Gdn:HCl denaturation characteristics are essentially identical for 3MP-α_3C and 2MP-α_3C and these proteins are 0.6 kcal mol^{-1} less stable than 4MP-α_3C. We conclude that all of the protein experimental data suggests that the "phenol rotation strategy" worked as intended and that the phenol OH group is solvent exposed in 4MP-α_3C and buried in more hydrophobic sites in 3MP-α_3C and 2MP-α_3C. Simple distance arguments are consistent with this notion. The α_3W

protein has a roughly cylindrical shape with a long axis of about 20 Å and a diameter of about 12 Å, with the Trp side chain located within the core of the protein (*48*). In α_3C, where the Cys side chain is expected to be located in a similar position near the central axis of the protein, the Cys sulfur will be about 6 Å from the protein surface. Geometry optimized MP-bCys models predict a distance from the cysteine sulfur atom to the phenol oxygen atom in 4MP-bCys to be 6.7 Å. The same distance is calculated to be 4.8 and 3.4 Å for the trans and cis conformations of 2MP-bCys, respectively. Thus, the phenol hydroxyl group in 4MP-α_3C could reside at the protein surface (>6 Å from the protein central axis) without significantly disrupting the main hydrophobic contact surfaces between the helices. In 2MP-α_3C, where the sulfur−oxygen distance is <6 Å, the OH group cannot reside at the protein surface without significantly disrupting the packing of the residues within the core of the protein, and the 2MP OH group thus most likely resides in a buried position.

The E_{peak} vs pH plots of 3MP-α_3C (Figure 7B) and 2MP-α_3C (Figure 7C) display a pH dependence across the pH 4 to 10 range. For the two proteins, and the bCys solution reference compounds at pH below their pK_{red} values, the slopes are within error to the predicted 59 mV/pH unit for a $1e^-/1H^+$ redox reaction (Table 2). Accordingly, the relevant redox pair to discuss for these two proteins is the PhO$^\bullet$/PhOH couple. Properties that may affect the potential of the neutral PhO$^\bullet$/PhOH redox pair of a protein-bound phenol include the hydrogen-bonding status of the reduced phenol, the hydrogen-bonding status of the phenoxyl radical, the fate of the phenolic proton and its associated charge upon formation of the neutral radical, and potential redox-induced structural changes occurring in the protein. We will start by discussing the two latter situations, and then address the hydrogen-bonding issues.

Itoh et al. reported that 2-methylthio-4-methylphenol has an E_{peak}(PhO$^\bullet$/PhO$^-$) about 100 mV lower than 4-methylphenol (*p*-cresol) and attributed the observed drop in potential to the electron-donating nature of the sulfur atom and to a stabilizing delocalization of the radical spin onto the sulfur giving the S−C_{ortho} link some double bond character (*63*, *64*). A number of experimental (*11*, *65*) and theoretical (*65*−*70*) studies have been performed on galactose oxidase and related model systems to investigate the electron magnetic resonance spectral properties and the spin-density distribution of the radical state. These studies show that the odd-alternate pattern, with large positive spin densities on the oxygen and the 2, 4, and 6 carbons and small negative densities on the 1, 3, and 5 carbons, typical of tyrosyl radicals is preserved in the sulfur-substituted systems. Some spin is distributed onto the sulfur atom although uncertainty remains with respect to the amount with values in the literature ranging from 0.03 (*68*) to 0.11−0.15 (*66*, *67*, *70*) to 0.28 (*65*).

The MP compounds investigated here differ from those cited above since the sulfur connected to the phenol ring is involved in an S−S bond. Nonetheless, if spin redistribution occurs, we would expect that situation for the 2MP and 4MP radicals, but not for the 3MP species. The E_{peak}(PhO$^\bullet$/PhO$^-$) of 3MP-bCys is +0.79 V, which is 0.10 and 0.15 V higher than the corresponding 2MP-bCys and 4MP-bCys values, respectively (Table 2). This increase in potential may to some extent reflect a lack of resonance stabilization in 3MP-bCys relative to the 2MP-bCys and 4MP-bCys compounds. If spin migration occurs in the 2- and/or 4MP system, structural changes could be coupled to redox change when the phenol is buried inside a protein matrix. This predicts an increase in the E_{peak} values of 2MP-α_3C and 4MP-α_3C relative to 2MP-bCys and 4MP-bCys. Contrary to this prediction, we observe an increase in potential for 2MP-α_3C and 3MP-α_3C, relative to 2MP-bCys and 3MP-bCys, and we detect no difference in the E_{peak}(PhO$^\bullet$/PhO$^-$) value for 4MP bound to the protein relative to the solvated compound. Although we cannot exclude structural changes occurring in 2MP-α_3C due to resonance stabilization, we find it unlikely since the predicted changes for the MP systems directly oppose the experimentally observed ones.

Electrochemical oxidation of 3MP-α_3C and 2MP-α_3C displays a 59 mV/pH unit dependence, which means that the proteins remain charge neutral in their oxidized state. The most reasonable conclusion from these data is that charge is not a significant parameter involved in raising the phenol potential in these systems. With respect to the mechanism of proton release from a radical site (*10*, *71*), it can be a direct transfer of the phenolic proton into the bulk solvent or a chain/web release, e.g., the phenolic proton is transferred to a primary acceptor which deprotonates from a second site to a buffer ion which, in turn, delivers the proton to a hydroxide ion in the bulk medium. For both these situations, the protonic charge is removed from the radical site and there is no energy penalty arising from solvating a charge inside the protein. A third possibility is that the observed proton release represents an electrostatic mechanism in which the protonic charge remains in the radical site. The resulting electrostatic field propagates through the protein matrix and shifts pK_A values of nearby amino acids with partial deprotonation occurring at several sites amounting to a total release of one proton. For 4MP-α_3C with its exposed OH group, the mechanism must be a direct transfer of the phenolic proton to molecules in the surrounding aqueous buffer. For both 3MP-α_3C and 2MP-α_3C there is some distance between the phenol hydroxyl group and the bulk medium suggesting a chain/web or an electrostatic release mechanism. Considering the clear 59 mV/pH unit dependence over 6 pH units as well as the small size of the labeled α_3C proteins, we find it most likely that the radical site equilibrates with the bulk medium on the time scale of the DPV experiment and that the observed proton release represents chain/web release rather than electrostatically driven deprotonation reactions.

When the OH group resides at or on the outside of the protein surface, the phenol redox properties are essentially identical for the protein as for the solution system (Figure 7A; Table 2). In contrast, when the OH group of the ligated phenol resides inside the protein, the phenol potential increases by 0.11−0.12 V relative to the solution values (Figure 7B,C; Table 2). As discussed above, we find it unlikely that the observed increase in potential is due to electrostatic interactions since the protein remains charge neutral upon oxidation. This suggests that differences in hydrogen bonding between the sequestered and solvent-exposed phenol OH group are the main parameter influencing the potential of the (PhO$^\bullet$/PhOH) redox couple. The higher potential measured for 3MP and 2MP when they are bound to α_3C relative to being free in solution predicts that the

protein hydrogen-bonding milieu stabilizes the reduced phenol species relative to the oxidized phenoxyl radical. Clearly the hydrogen-bonding environment, i.e., the number of hydrogen bonds, the strength of the interaction(s), and the identity of the hydrogen-bonding partner(s), will differ between the protein-bound and the solvated phenols. For the latter compounds, water is the dominating hydrogen-bonding partner. Phosphate buffer molecules could also be involved in hydrogen bonding, but their concentration (10 mM) is substantially less than the water concentration (55 M). A reduced phenol is a hydrogen-bonding donor while the neutral phenoxyl radical is a hydrogen-bonding acceptor and both redox states can be involved in more than one hydrogen bond (e.g., *45*, *72*, *73*). For freely dissolved phenol, the water molecules can easily reorient to form multiple hydrogen bonds to both the reduced and oxidized states. This is not expected to occur with the same ease when the phenol OH group is buried inside α_3C. As noted earlier, Leu, Ile, and Val residues form the main part of the hydrophobic core in α_3C and for this system potential hydrogen-bonding partners include sequestered water molecules and the protein backbone. It is also possible that the Glu residues residing in interhelical position could be involved in a hydrogen bond with the ligated phenol. For example in the structural model of 3MP-α_3C, the phenol oxygen is located 3.3 and 4.0 Å from the two oxygen atoms of Glu-35. Relative to solvated water molecules, these hydrogen-bonding partners are expected to be substantially less dynamic in terms of structural rearrangements in response to a redox change. For the 2MP-α_3C system, the situation is expected to be even more restricted with steric crowding of the phenol oxygen by the S-protein bond. In conclusion, hydrogen bonds between the protein matrix and the ligated phenols either stabilize the reduced phenol or destabilize the radical state, relative to the aqueous buffer system. This effect provides an increase in the E_{peak}(PhO•/PhOH) value of up to 0.11 V in 3MP-α_3C and 0.12 V in 2MP-α_3C. Future studies investigating the hydrogen-bonding properties of the reduced and oxidized states of the MP-α_3C proteins will provide more details on this issue.

CONCLUSIONS

The pK_A and E_{peak} values are essential identical when 4MP is ligated to α_3C relative to when it is free in aqueous buffer. In contrast, both the potential and the pK_A value increase in 3MP-α_3C and 2MP-α_3C relative to the solvated compounds. The E_{peak} vs pH plots of 3MP-α_3C and 2MP-α_3C, and of 4MP-α_3C in the acid range relative to the phenol pK_A, display a ~59 mV/pH unit dependence. This is consistent with a one-electron oxidation of the phenol to the neutral phenoxyl radical and the release of one full proton into the bulk medium. In 4MP-α_3C, hydrophobic core and charged surface residues fold around the phenol ring while its hydroxyl group is fully exposed to the solvent. The heterogeneous milieu surrounding the protein-ligated phenol differs distinctly from the homogeneous high-dielectric environment of the solvated 4MP compound, and yet their redox properties are remarkable similar. We conclude that interactions to the phenol OH group are dominating in determining the phenol redox characteristics and that the environment around the remaining part of the phenolic molecule has no significant impact. Neither charge not structural interactions appear to be involved in raising the phenol potential in 3MP-α_3C and 2MP-α_3C. The hydrogen-bonding milieu of the ligated phenols, relative to when these molecules are solvated in aqueous buffer, seems to be the main parameter raising their potentials in the protein.

ACKNOWLEDGMENT

We thank Drs. Josh Wand and Kathy Valentine for assistance with the NMR measurements. Mass spectrometry analyses were performed by the Protein Analysis Centre, the Karolinska Institute, Stockholm.

REFERENCES

1. Stubbe, J., and van der Donk, W. A. (1998) Protein radicals in enzyme catalysis, *Chem. Rev. 98*, 705−762.
2. Pesavento, R. P., and van der Donk, W. A. (2001) Tyrosyl radical cofactors, *Adv. Protein Chem. 58*, 317−385.
3. Himo, F., and Siegbahn, P. E. M. (2003) Quantum chemical studies of radical-containing enzymes, *Chem. Rev. 103*, 2421−2456.
4. Hoganson, C. W., and Tommos, C. (2004) The function and characteristics of tyrosyl radical cofactors, *Biochim. Biophys. Acta 1655*, 116−122.
5. Westerlund, K., Berry, B. W., Privett, H. K., and Tommos, C. (2005) Exploring amino-acid radical chemistry: protein engineering and de novo design, *Biochim. Biophys. Acta 1707*, 103−116.
6. Reichard, P., and Ehrenberg, A. (1983) Ribonucleotide reductase—a radical enzyme, *Science 221*, 514−519.
7. Eklund, H., Uhlin, U., Färnegårdh, M., Logan, D. T., and Nordlund, P. (2001) Structure and function of the radical enzyme ribonucleotide reductase, *Prog. Biophys. Mol. Biol. 77*, 177−268.
8. Stubbe, J., Nocera, D. G., Yee, C. S., and Chang, M. C. Y. (2003) Radical initiation in the class I ribonucleotide reductase: Long-range proton-coupled electron transfer?, *Chem. Rev. 103*, 2167−2201.
9. Babcock, G. T., Barry, B. A., Debus, R. J., Hoganson, C. W., Atamian, M., McIntosh, L., Sithole, I., and Yocum, C. F. (1989) Water oxidation in photosystem II: From radical chemistry to multielectron chemistry, *Biochemistry 28*, 9557−9565.
10. Tommos, C. (2002) Electron, proton and hydrogen-atom transfers in photosynthetic water oxidation, *Philos. Trans. R Soc. Lond. B Biol. Sci. 357*, 1383−1394.
11. Babcock G. T., El-Deeb M. K., Sandusky P. O., Whittaker M. M., and Whittaker J. W. (1992) Electron-paramagnetic resonance and electron nuclear double-resonance spectroscopies of the radical site in galactose-oxidase and of thioether-substituted phenol model compounds, *J. Am. Chem. Soc. 114*, 3727−3734.
12. Whittaker, M. M., Kersten, P. J., Nakamura, N., Sanders-Loehr, J., Schweizer, E. S., and Whittaker, J. W. (1996) Glyoxal oxidase from Phanerochaete chrysosporium is a new radical-copper oxidase, *J. Biol. Chem. 1271*, 681−687.
13. Whittaker, J. W. (2003) Free radical catalysis by galactose oxidase, *Chem. Rev. 103*, 2347−2363.
14. Proshlyakov, D. A., Pressler, M. A., DeMaso, C., Leykam, J. F., DeWitt, D. L., and Babcock, G. T. (2000) Oxygen activation and reduction in respiration: involvement of redox-active tyrosine 244, *Science 290*, 1588−1591.
15. Karthein, R., Dietz, R., Nastainczyk, W., and Ruf, H. H. (1988) Higher oxidation states of prostaglandin H synthase. EPR study of a transient tyrosyl radical in the enzyme during the peroxidase reaction, *Eur. J. Biochem. 171*, 313−320.
16. Tsai, A.-L., and Kulmacz, R. J. (2000) Tyrosyl radicals in prostaglandin H synthase-1 and -2, *Prostaglandins Other Lipid Mediators 62*, 231−254.
17. Wilson, J. C., Wu, G., Tsai, A. L., and Gerfen, G. J. (2005) Determination of the structural environment of the tyrosyl radical in prostaglandin H-2 synthase-1: A high-frequency ENDOR/EPR study, *J. Am. Chem. Soc. 127*, 1618−1619.
18. Ivancich, A., Jouve, H. M., and Gaillard, J. (1996) EPR evidence for a tyrosyl radical intermediate in bovine liver catalase, *J. Am. Chem. Soc. 118*, 12852−12853.
19. Su, C., Sahlin, M., and Oliw, E. H. (1998) A protein radical and ferryl intermediates are generated by linoleate diol synthase, a ferric hemeprotein with dioxygenase and hydroperoxide isomerase activities, *J. Biol. Chem. 273*, 20744−20751.

20. Ivancich, A., Mazza, G., and Desbois, A. (2001) Comparative electron paramagnetic resonance study of radical intermediates in turnip peroxidase isozymes, *Biochemistry 40*, 6860−6866.
21. Chouchane S., Girotto S., Yu, S. W., and Magliozzo R. S. (2002) Identification and characterization of tyrosyl radical formation in *Mycobacterium tuberculosis* catalase-peroxidase (KatG), *J. Biol. Chem. 277*, 42633−42638.
22. Ivancich, A., Jakopitsch, C., Auer, M., Un, S., and Obinger, C. (2003) Protein-based radicals in the catalase-peroxidase of *Synechocystis* PCC6803: A multifrequency EPR investigation of wild-type and variants on the environment of the heme active site, *J. Am. Chem. Soc. 125*, 14093−14102.
23. Schunemann, V., Lendzian, F., Jung, C., Contzen, J., Barra, A. L., Sligar, S. G., and Trautwein, A. X. (2004) Tyrosine radical formation in the reaction of wild type and mutant cytochrome P450cam with peroxy acids−A multifrequency EPR study of intermediates on the millisecond time scale, *J. Biol. Chem. 279*, 10919−10930.
24. Aubert, C., Mathis, P., Eker, A. P. M., and Brettel, K. (1999) Intraprotein electron transfer between tyrosine and tryptophan in DNA photolyase from *Anacystis nidulans*, *Proc. Natl. Acad. Sci. U.S.A. 96*, 5423−5427.
25. Aubert, C., Brettel, K., Mathis, P., Eker, A. P. M., and Boussac, A. (1999) EPR detection of the transient tyrosyl radical in DNA photolyase from *Anacystis nidulans*, *J. Am. Chem. Soc. 121*, 8659−8660.
26. Giovani, B., Byrdin, M., Ahmad, M., and Brettel, K. (2003) Light-induced electron transfer in a cryptochrome blue-light photoreceptor, *Nat. Struct. Biol. 10*, 489−490.
27. Rigby, S. E. J., Hynson, R. M. G., Ramsay, R. R., Munro, A. W., and Scrutton, N. S. (2005) A stable tyrosyl radical in monoamine oxidase A, *J. Biol. Chem. 280*, 4627−4631.
28. Vass, I., and Styring, S. (1991) pH-dependent charge equilibria between tyrosine-D and the S states in photosystem II. Estimation of relative midpoint redox potentials, *Biochemistry 30*, 830−839.
29. Silva, K. E., Elgren, T. E., Que, L., and Stankovich, M. T. (1995) Electron-transfer properties of the R2 protein of ribonucleotide reductase from *Escherichia coli*, *Biochemistry 34*, 14093−14103.
30. Saysell, C. G., Borman, C. D., Baron, A. J., McPherson, M. J., and Sykes, A. G. (1997) Kinetic studies on the redox interconversion of $GOase_{semi}$ and $GOase_{ox}$ forms of galactose oxidase with inorganic complexes as redox partners, *Inorg. Chem. 36*, 4520−4525.
31. Saysell, C. G., Barna, T., Borman, C. D., Baron, A. J., McPherson, M. J., and Sykes, A. G. (1997) Properties of the Trp290His variant of *Fusarium* NRRL 2903 galactose oxidase: interactions of the $GOase_{semi}$ state with different buffers, its redox activity and ability to bind azide, *J. Biol. Inorg. Chem. 2*, 702−709.
32. Wright, C., and Sykes, A. G. (2001) Interconversion of Cu^{I} and Cu^{II} forms of galactose oxidase: comparison of reduction potentials, *J. Inorg. Biochem. 85*, 237−243.
33. Ito, N., Phillips, S. E. V., Stevens, C., Ogel, Z. B., McPherson, M. J., Keen, J. N., Yadav, K. D. S., and Knowles, P. F. (1991) Novel thioether bond revealed by a 1.7 Å crystal structure of galactose oxidase, *Nature 350*, 87−90.
34. Ito, N., Phillips, S. E. V., Stevens, C., Ogel, Z. B., McPherson, M. J., Keen, J. N., Yadav, K. D. S., and Knowles, P. F. (1992) Three-dimensional structure of galactose oxidase: an enzyme with a built-in secondary cofactor, *Faraday Discuss. 93*, 75−84.
35. Ito, N., Phillips, S. E. V., Yadav, K. D. S., and Knowles, P. F. (1994) Crystal structure of a free radical enzyme, galactose oxidase, *J. Mol. Biol. 238*, 794−814.
36. Tommos, C., Skalicky, J. J., Pilloud, D. L., Wand, A. J., and Dutton, P. L. (1999) De novo proteins as models of radical enzymes, *Biochemistry 38*, 9495−9507.
37. Tommos, C., and Babcock, G. T. (2000) Proton and hydrogen currents in photosynthetic water oxidation, *Biochim. Biophys. Acta 1458*, 199−219.
38. Diner, B. A. (2001) Amino acid residues involved in the coordination and assembly of the manganese cluster of photosystem II. Proton-coupled electron transport of the redox-active tyrosines and its relationship to water oxidation, *Biochim. Biophys. Acta 1503*, 147−163.
39. Debus, R. J. (2001) Amino acid residues that modulate the properties of tyrosine Y_Z and the manganese cluster in the water oxidizing complex of photosystem II, *Biochim. Biophys. Acta 1503*, 164−186.
40. Faller, P., Goussias, C., Rutherford, A. W., and Un, S. (2003) Resolving intermediates in biological proton-coupled electron transfer: A tyrosyl radical prior to proton movement, *Proc. Natl. Acad. Sci. U.S.A. 100*, 8732−8735.
41. Maki, T., Araki, Y., Ishida, Y., Onomura, O., and Matsumura, Y. (2001) Construction of persistent phenoxyl radical with intramolecular hydrogen bonding, *J. Am. Chem. Soc. 123*, 3371−3371.
42. Benisvy, L., Blake, A. J., Collison, D., Davies, E. S., Garner, C. D., McInnes, E. J. L., McMaster, J., Whittaker, G., and Wilson, C. (2003) A phenol-imidazole pro-ligand that can exist as a phenoxyl radical, alone and when complexed to copper(II) and zinc(II), *Dalton Trans. 10*, 1975−1985.
43. Thomas, F., Jarjayes, O., Jamet, M., Hamman, S., Saint-Aman, E., Duboc, C., and Pierre, J. L. (2004) How single and bifurcated hydrogen bonds influence proton-migration rate constants, redox, and electronic properties of phenoxyl radicals, *Angew. Chem., Int. Ed. 43*, 594−597.
44. Rhile, I. J., and Mayer, J. M. (2004) One-electron oxidation of a hydrogen-bonded phenol occurs by concerted proton-coupled electron transfer, *J. Am. Chem. Soc. 126*, 12718−12719.
45. Lucarini, M., Mugnaini, V., Pedulli, G. F., and Guerra, M. (2003) Hydrogen-bonding effects on the properties of phenoxyl radicals. An EPR, kinetic, and computational study, *J. Am. Chem. Soc. 125*, 8318−8329.
46. Di Bilio, A. J., Crane, B. R., Wehbi, W. A., Kiser, C. N., Abu-Omar, M. M., Carlos, R. M., Richards, J. H., Winkler, J. R., and Gray, H. B. (2001) Properties of photogenerated tryptophan and tyrosyl radicals in structurally characterized proteins containing rhenium(I) tricarbonyl diimines, *J. Am. Chem. Soc. 123*, 3181−3182.
47. Narváez, A. J., LoBrutto, R., Allen, J. P., and Williams, J. C. (2004) Trapped tyrosyl radical populations in modified reaction centers from *Rhodobacter sphaeroides*, *Biochemistry 43*, 14379−14384.
48. Dai, Q.-H., Tommos, C., Fuentes, E. J., Blomberg, M. R. A., Dutton, P. L., and Wand, A. J. (2002) Structure of a de novo designed protein model of radical enzymes, *J. Am. Chem. Soc. 124*, 10952−10953.
49. Ellman, G. L. (1959) Tissue sulfhydryl groups. *Arch. Biochem. Biophys. 82*, 70−77.
50. Santoro, M. M., and Bolen, D. W. (1988) Unfolding free energy changes determined by the linear extrapolation method. 1. Unfolding of phenylmethanesulfonyl alpha-chymotrypsin using different denaturants, *Biochemistry 27*, 8063−8068.
51. Betz, S., Fairman, R., O'Neil, K., Lear, J., and Degrado, W. (1995) Design of 2-stranded and 3-stranded coiled-coil peptides, *Philos. Trans. R. Soc. London, Ser. B 348*, 81−88.
52. Pace, C. N., and Scholtz, J. M. (1998) A helix propensity scale based on experimental studies of peptides and proteins, *Biophys. J. 75*, 422−427.
53. Yee, C. S., Seyedsayamdost, M. R., Chang, M. C. Y., Nocera, D. G., and Stubbe, J. (2003) Generation of the R2 subunit of ribonucleotide reductase by intein chemistry: Insertion of 3-nitrotyrosine at residue 356 as a probe of the radical initiation process, *Biochemistry 42*, 14541−14552.
54. Yee, C. S., Chang, M. C. Y., Ge, J., Nocera, D. G., and Stubbe, J. (2003) 2,3-Difluorotyrosine at position 356 of ribonucleotide reductase R2: A probe of long-range proton-coupled electron transfer, *J. Am. Chem. Soc. 125*, 10506−10507.
55. Chang, M. C. Y., Yee, C. S., Nocera, D. G., and Stubbe, J. (2004) Site-specific replacement of a conserved tyrosine in ribonucleotide reductase with an aniline amino acid: A mechanistic probe for a redox-active tyrosine, *J. Am. Chem. Soc. 126*, 16702−16703.
56. Sjödin, M., Styring, S., Wolpher, H., Xu, Y. H., Sun, L. C., and Hammarström, L. (2005) Switching the redox mechanism: Models for proton-coupled electron transfer from tyrosine and tryptophan, *J. Am. Chem. Soc. 127*, 3855−3863.
57. Surdhar, P. S., and Armstrong, D. A. (1987) Reduction potentials and exchange reactions of thiyl radicals and disulfide anion radicals, *J. Phys. Chem. 91*, 6532−6537.
58. Schreyer, S. K., and Mikkelsen, S. R. (1999) A synthetic cysteine oxidase based on a ferrocene-cyclodextrin conjugate, *Bioconjugate Chem. 10*, 464−469.
59. Ralph, T. R., Hitchman, M. L., Millington, J. P., and Walsh, F. C. (1994) The electrochemistry of L-cystine and L-cysteine: part 1: thermodynamic and kinetic studies, *J. Electroanal. Chem. 375*, 1−15.
60. Parry, E. P., and Osteryoung, R. A. (1965) Evaluation of Analytical Pulse Polarography, *Anal. Chem. 37*, 1634−1637.
61. Harriman, A. (1987) Further comments on the redox potentials of tryptophan and tyrosine, *J. Phys. Chem. 91*, 6102−6104.

62. DeFelippis, M. R., Murthy, C. P., Broitman, F., Weinraub, D., Faraggi, M., and Klapper, M. H. (1991) Electrochemical properties of tyrosine phenoxy and tryptophan indolyl radicals in peptides and amino acid analogs, *J. Phys. Chem. 95*, 3416−3419.
63. Itoh, S., Hirano, K., Furuta, A., Konatsu, M., Oshiro, Y., Ishida, A., Takamuku, S., Kohzuma, Y., Nakamura, N., and Suzuki, S. (1993) Physicochemical properties of 2-methylthio-4-methylphenol, a model compound of the novel cofactor in galactose oxidase, *Chem. Lett. 22*, 2099−2102.
64. Itoh, S., Takayama, S., Arakawa, R., Furuta, A., Komatsu, M., Ishida, A., Takamuku, S., and Fukuzumi, S. (1997) Active site models for galactose oxidase. Electronic effect of the thioether group in the novel organic cofactor, *Inorg. Chem. 36*, 1407−1416.
65. Gerfen, G. J., Bellew, B. F., Griffin, R. G., Singel, D. J., Ekberg, C. A., and Whittaker, J. W. (1996) High-frequency electron paramagnetic resonance spectroscopy of the apogalactose oxidase radical, *J. Phys. Chem. 100*, 16739−16748.
66. Wise, K. E., Pate, J. B., and Wheeler, R. A. (1999) Phenoxyl, (methylthio)phenoxyl, and (methylthio)cresyl radical models for the structures, vibrations, and spin properties of the cysteine-linked tyrosyl radical in galactose oxidase, *J. Phys. Chem. B 103*, 4764−4772.
67. Himo, F., Babcock, G. T., and Eriksson, L. A. (1999) Tyrosyl radical in galactose oxidase not strongly perturbed by cysteine cross-link, *Chem. Phys. Lett. 313*, 374−378.
68. Engström, M., Himo, F., and Ågren, H. (2000) Ab initio *g*-tensor calculations of the thioether substituted tyrosyl radical in galactose oxidase, *Chem. Phys. Lett. 319*, 191−196.
69. Boulet, A. M., Walter, E. D., Schwartz, D. A., Gerfen, G. J., Callis, P. R., and Singel, D. J. (2000) Electronic structure and hyperfine interactions in thioether-substituted tyrosyl radicals, *Chem. Phys. Lett. 331*, 108−114.
70. Kaupp, M., Gress, T., Reviakine, R., Malkina, O. L., and Malkin, V. G. (2003) *g* tensor and spin density of the modified tyrosyl radical in galactose oxidase: A density functional study, *J. Phys. Chem. B 107*, 331−337.
71. Junge, W., Haumann, M., Ahlbrink, R., Mulkidjanian, A., and Clausen, J. (2002) Electrostatics and proton transfer in photosynthetic water oxidation, *Philos. Trans. R Soc. Lond. B Biol. Sci. 357*, 1407−1417.
72. Chipman, D. M. (2000) Hydrogen-bonding effects on free-radical properties, *J. Phys. Chem. A 104*, 11816−11821.
73. Guerra, M., Amorati, R., and Pedulli, G. F. (2004) Water effect on the O−H dissociation enthalpy of para-substituted phenols: a DFT study, *J. Org. Chem. 69*, 5460−5467.
74. Guex, N., and Peitsch, M. C. (1997) Swiss-model and the Swiss-PdbViewer: An environment for comparative protein modeling, *Electrophoresis 18*, 2714−2723.
75. Sönnichsen, F. D., Van Eyk, J. E., Hodges, R. S., and Sykes, B. D. (1992) Effect of trifluoroethanol on protein secondary structure: an NMR and CD study using a synthetic actin peptide, *Biochemistry 31*, 8790−8798.
76. Chen, Y.-H., Yang, J.-T., and Chau, K. H. (1974) Determination of the helix and β form of proteins in aqueous solvents by circular dichroism, *Biochemistry 13*, 3350−3359.

BI050901Q